

Paul G. Leonard,<sup>a</sup>‡ Gary N.  
Parkinson,<sup>b</sup> Jayesh Gor,<sup>a</sup>  
Stephen J. Perkins<sup>a</sup> and  
John E. Ladbury<sup>a\*</sup>§

<sup>a</sup>Department of Structural and Molecular  
Biology, University College London,  
Gower Street, London WC1E 6BT, England, and  
<sup>b</sup>Cancer Research UK Biomolecular Structure  
Group, The School of Pharmacy,  
University of London, 29-39 Brunswick Square,  
London WC1N 1AX, England

‡ Present address: Center of Advanced  
Biotechnology and Medicine, University of  
Medicine and Dentistry of New Jersey,  
679 Hoes Lane, Piscataway, NJ 08854, USA.

§ Present address: University of Texas  
M. D. Anderson Cancer Center, Unit 1000,  
1515 Holcombe Boulevard, Houston,  
TX 77030, USA.

Correspondence e-mail:  
jeladbury@mdanderson.org

Received 4 January 2010  
Accepted 4 February 2010

## The absence of inorganic salt is required for the crystallization of the complete oligomerization domain of *Salmonella typhimurium* histone-like nucleoid-structuring protein

The histone-like nucleoid-structuring protein (H-NS) plays an important role in both DNA packaging and global gene regulation in enterobacteria. Self-association of the N-terminal domain results in polydisperse oligomers that are critical to the function of the protein. This heterogeneity in oligomer size has so far prevented structure determination of the complete oligomerization domain by NMR or X-ray crystallography. In the absence of inorganic salt, the H-NS oligomerization domain is predominantly restricted to an equilibrium between a homodimer and homotetramer, allowing a protein solution to be prepared that is sufficiently homogeneous for successful crystallization. Crystallization was achieved by tailoring the conditions screened to those identified as minimizing the potential disruption of protein-solution homogeneity. This finding provides a significant step towards resolving the structure of this important prokaryotic protein.

### 1. Introduction

The histone-like nucleoid-structuring protein (H-NS) is a major component of protein-mediated chromatin condensation and functions as a global regulator of transcription in enteric bacteria (Dorman, 2004; Rimsky, 2004), playing an important role in regulating gene expression in response to environmental stresses such as temperature change (Ono *et al.*, 2005; White-Ziegler & Davis, 2009), osmotic stress, pH change and oxygen availability (Hommais *et al.*, 2001). H-NS acts as a repressor of gene expression, silencing specific genes or regions of the chromosome either in concert (Browning *et al.*, 2000) or in an antagonistic manner with other transcription factors and nucleoid-associated proteins (Dame & Goosen, 2002; De la Cruz *et al.*, 2007; Falconi *et al.*, 2001).

The H-NS protein consists of two functional domains, an N-terminal oligomerization domain (Met1–Lys83) and a C-terminal DNA-binding domain (Ala91–Glu137), separated by a short linker (Dorman *et al.*, 1999; Leonard *et al.*, 2009). The N-terminal oligomerization domain self-associates to form homodimers and larger oligomeric species (Smyth *et al.*, 2000) and additionally interacts with several other proteins in the cytosol which modulate the size and function of the H-NS complex (Johansson *et al.*, 2001; Nieto *et al.*, 2002; Williamson & Free, 2005). Two structures of truncated forms of the oligomerization domain have been solved by NMR which share common secondary-structure elements but differ in the alignment of the  $\alpha$ -helices in the homodimer structures. The N-terminal 47 residues of the H-NS protein adopt an antiparallel coiled-coil configuration (Bloch *et al.*, 2003), whereas the N-terminal 58 residues of H-NS form a parallel coiled coil (Esposito *et al.*, 2002). Whilst the two NMR structures give useful insight into the coiled-coil dimerization interface, they provide little information about how the intact protein can form high-order complexes as approximately a third of the oligomerization domain is not included in these structures. In particular, the residues between Leu65 and Asn77 are known to be essential for the oligomerization of H-NS homodimers to form larger complexes (Leonard *et al.*, 2009).

In this report, we demonstrate that after identifying solution conditions that create a more homogeneous protein population, a biased crystallization screen, avoiding conditions known to generate heterogeneous oligomeric states, can be used to identify crystallization conditions of the complete H-NS oligomerization domain.

## 2. Materials and methods

### 2.1. Protein expression and purification

The *Salmonella typhimurium* H-NS<sub>1-83</sub> C21S protein was expressed and purified as described previously (Leonard *et al.*, 2009). Briefly, the H-NS<sub>1-83</sub> C21S protein was expressed in *Escherichia coli* with an N-terminal His<sub>6</sub>-tag fusion. After purification of the protein using a Talon metal-affinity resin column, the His<sub>6</sub>-tag was proteolytically cleaved by thrombin. The His<sub>6</sub>-tags and any uncleaved protein were captured on the Talon column prior to further purification of H-NS<sub>1-83</sub> C21S by Q-Sepharose anion-exchange chromatography followed by Superdex 75 gel-filtration chromatography. The three amino acids glycine, serine and histidine remain N-terminal to the H-NS<sub>1-83</sub> C21S protein after cleavage of the His<sub>6</sub>-tag. The mutation of Cys21 to a serine does not affect the self-association of H-NS (Smyth

*et al.*, 2000), but prevents erroneous dimerization through disulfide-bond formation.

### 2.2. Analytical ultracentrifugation

All analytical ultracentrifugation (AUC) experiments were performed at 293 K using a Beckman XL-I instrument equipped with an AnTi50 rotor set to record both interference scans and 280 nm absorbance scans. Sedimentation-velocity AUC data for H-NS<sub>1-83</sub> C21S were acquired over 16 h at a rotor speed of 35 000 rev min<sup>-1</sup>. The experiments were performed in two-sector cells with 12 mm column height loaded with 400 µl of either protein or reference buffer solution. Successive scans were recorded at 9 min intervals for both 280 nm absorbance and interference measurements. The sedimentation boundaries were fitted to a sedimentation-coefficient distribution  $c(S)$  derived from the Lamm equation calculated using the program *SEDPHAT* (Schuck, 2000). 200 sedimentation-coefficient increments were used between 0.5 and 3 S for the analysis, with the Tikhonov regularization parameter set to 0.95. The frictional ratio was allowed to float during fitting. The  $c(S)$  distributions were normalized to account for differences in the amount of protein present in the sample by dividing the  $y$  values obtained by the total intensity in the  $c(S)$  distribution.

Sedimentation-equilibrium AUC analysis was performed over a period of 30 h at each rotor speed using six-sector cells with 2 mm column heights. 100 µl samples containing 500, 250, 63 and 31 µM H-NS<sub>1-83</sub> C21S in 20 mM MOPS pH 7.0 were monitored until equilibrium was reached, as shown by the perfect overlay of scans recorded at 3 h intervals, at rotor speeds of 19 000, 22 000 and 26 000 rev min<sup>-1</sup>. The sedimentation profiles were fitted to a model for an H-NS<sub>1-83</sub> C21S homodimer and homotetramer equilibrium using *SEDPHAT* (Schuck, 2000). The molar masses were fixed at 19 566 and 39 132 g mol<sup>-1</sup> and the association constant and cell-bottom position were optimized by nonlinear regression. The calculated partial specific volume,  $\bar{v}$ , for H-NS<sub>1-83</sub> C21S of 0.7312 ml g<sup>-1</sup> was determined using *SEDNTERP* (Laue *et al.*, 1992). The solvent density,  $\rho$ , of 0.999671 g cm<sup>-3</sup> was measured using a DMA5000

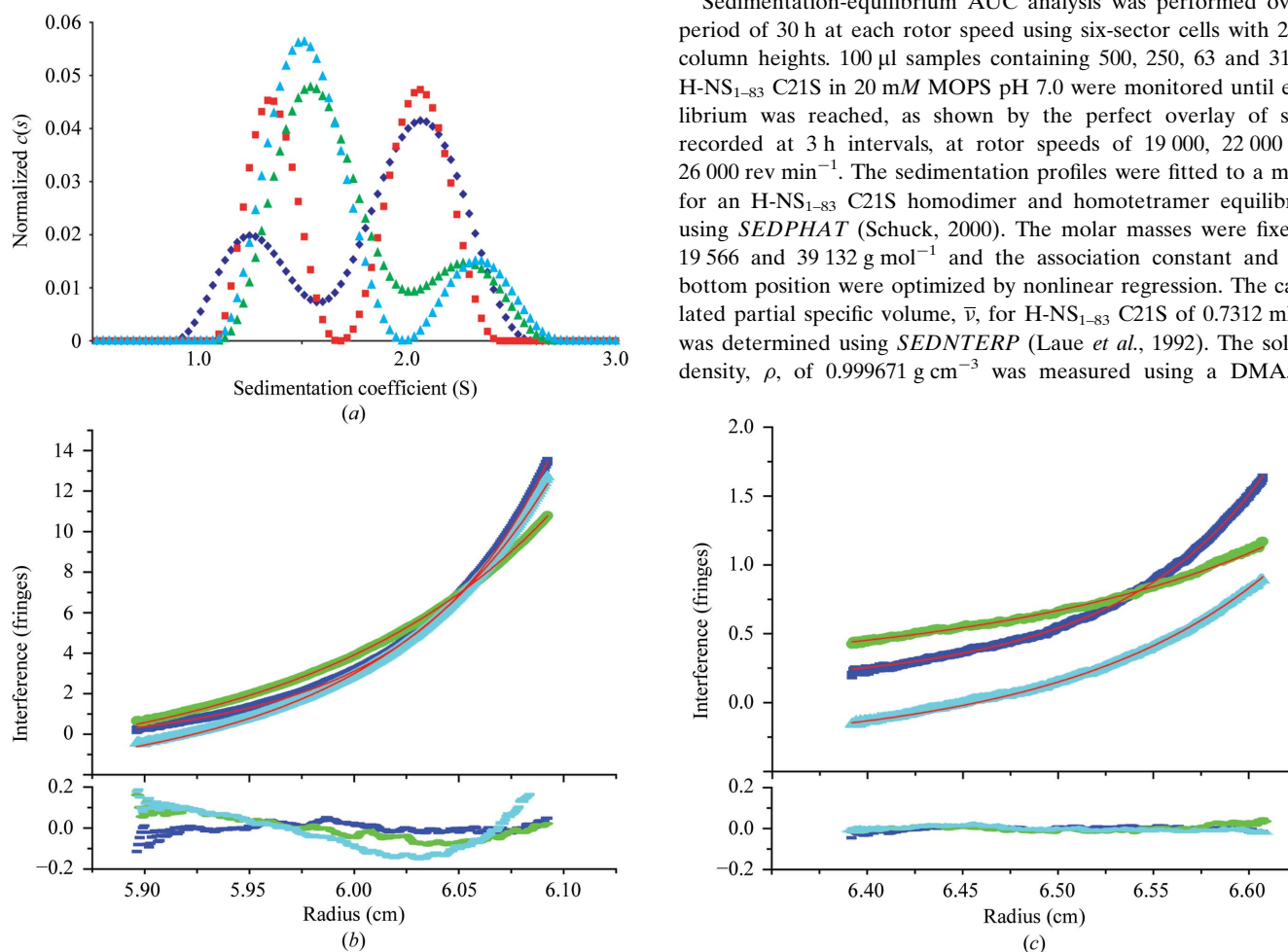


**Figure 1** Analytical ultracentrifugation analysis of H-NS<sub>1-83</sub> C21S in 20 mM MOPS pH 7.0 at 293 K. (a) The  $c(S)$  distributions determined from sedimentation-velocity AUC experiments with 559 µM H-NS<sub>1-83</sub> C21S (blue), 281 µM H-NS<sub>1-83</sub> C21S (red), 132 µM H-NS<sub>1-83</sub> C21S (green) and 69 µM H-NS<sub>1-83</sub> C21S (cyan). The  $c(S)$  distributions were normalized to account for the different amounts of total protein present in each sample. (b, c) Sedimentation-equilibrium AUC profiles of H-NS<sub>1-83</sub> C21S recorded at 19 000 rev min<sup>-1</sup> (green), 22 000 rev min<sup>-1</sup> (cyan) and 26 000 rev min<sup>-1</sup> (blue). The solid red lines superimposed onto the raw data correspond to the nonlinear regression fits for a dimer-to-tetramer equilibrium model using the *SEDPHAT* software (Schuck, 2000). Interference versus radius curves are shown for (b) 500 µM and (c) 31 µM starting concentrations of H-NS<sub>1-83</sub> C21S. The residuals for the fit are shown below each data set.

densitometer (Anton Paar). The solvent viscosity  $\eta$  was taken to be  $0.0010164 \text{ Pa s}^{-1}$  based on an assumption that the viscosity of 20 mM MOPS is the same as the established viscosity of 20 mM HEPES (Laue *et al.*, 1992).

### 2.3. Protein crystallization and data collection

Crystallization conditions for H-NS<sub>1-83</sub> C21S were initially screened using a microbatch setup incubated at 289 K. 5 ml paraffin oil was used to cover all 72 wells of a Terasaki plate. 1  $\mu\text{l}$  of the crystallization solution was then dispensed into a well and mixed with 1  $\mu\text{l}$  2 mM H-NS<sub>1-83</sub> C21S in 20 mM MOPS pH 7.0. Hanging drops were additionally prepared in 24-well pre-greased VDX plates (Hampton Research) with 1 ml reservoir solution. The hanging drop was prepared by mixing 1  $\mu\text{l}$  reservoir solution with 1  $\mu\text{l}$  H-NS<sub>1-83</sub> C21S (2 mM in 20 mM MOPS pH 7.0).

All crystals were flash-cooled after a 1 min soak in 50 mM MES, 12% (v/v) MPD, 10 mM phenol, 20% (v/v) glycerol pH 6.2. Data were collected from a native crystal on the European Synchrotron Radiation Facility (ESRF) beamline ID23-2 equipped with a MAR Mosaic 225 detector. The crystal was exposed for 2 s at a crystal-to-detector distance of 371 mm with a  $1^\circ$  oscillation. 75 images were collected. Processing and data reduction were performed using *d\*TREK* (Pflugrath, 1999).

## 3. Results and discussion

### 3.1. Self-association of H-NS<sub>1-83</sub> C21S under low ionic strength conditions

The H-NS<sub>1-83</sub> C21S protein contains all the necessary amino acids for the formation of homodimers and larger oligomeric species, demonstrating that this protein is the fully functional oligomerization domain (Leonard *et al.*, 2009). Lowering the salt concentration has been shown to disrupt the self-association of H-NS<sub>1-83</sub> C21S, shifting the equilibrium towards smaller species (Leonard *et al.*, 2009). At low salt concentrations there are insufficient ions present in the solution to shield like-charge repulsion forces between the H-NS molecules, causing a shift in the size distribution towards the smaller oligomeric states. Therefore, low ionic strength solvent conditions provide us with a unique opportunity to identify buffer conditions in which the protein sample should be sufficiently homogeneous for crystallization. Samples of H-NS<sub>1-83</sub> C21S dissolved in 20 mM MOPS pH 7.0 without any additional salt were analysed using sedimentation-velocity AUC (Fig. 1*a*). At loading concentrations of 69  $\mu\text{M}$  and 132  $\mu\text{M}$  H-NS<sub>1-83</sub> C21S the majority of the protein corresponds to a species with a sedimentation coefficient of 1.6 S, with a second species present at 2.4 S. When 281  $\mu\text{M}$  H-NS<sub>1-83</sub> C21S was loaded into the sample cell, approximately half of the protein corresponds to the smaller species and half of the protein is now present as the larger species, suggesting that this protein concentration is close to the dissociation constant for this equilibrium. A further increase in protein concentration to 559  $\mu\text{M}$  shifts the distribution in favour of the larger species. At the higher concentrations of 281 and 559  $\mu\text{M}$  H-NS<sub>1-83</sub> C21S the peaks observed in the  $c(S)$  distribution are shifted towards lower sedimentation coefficients relative to the position of the peaks in the  $c(S)$  distribution for 69 and 132  $\mu\text{M}$  H-NS<sub>1-83</sub> C21S because of the non-ideal solution conditions found at high protein concentrations. At high protein concentrations the viscosity of the solution increases and charge-repulsion forces are observed between the protein molecules as the centrifugal force pulls the protein towards the bottom of the centrifuge cell. Hence, slower sedi-

mentation of the protein is observed than expected for the same protein species sedimenting under dilute conditions.

Sedimentation-equilibrium AUC analysis was performed using the same solvent conditions (20 mM MOPS pH 7.0) with loaded protein concentrations of H-NS<sub>1-83</sub> C21S from 31 to 500  $\mu\text{M}$  protein at three rotor speeds of 19 000, 22 000 and 26 000  $\text{rev min}^{-1}$  (Figs. 1*b* and 1*c*). A model for a homodimer-to-homotetramer equilibrium gave the best agreement with the distribution observed in the sedimentation-velocity data. The dissociation constant was allowed to float in the analysis, but the molar masses of the two protein species were fixed at 19 566.2 and 39 132.4  $\text{g mol}^{-1}$ , the calculated molar masses of an H-NS<sub>1-83</sub> C21S dimer and tetramer, respectively. The best fit gives a dissociation constant of  $260 \pm 60 \mu\text{M}$  for a dimer-to-tetramer equilibrium, which is in good agreement with the sedimentation-velocity  $c(S)$  distributions observed under the same solvent conditions. Attempts to fit the sedimentation-equilibrium curves to alternative models (dimer-trimer equilibrium, dimer-pentamer equilibrium, dimer-hexamer equilibrium) did not produce fits with a dissociation constant that was consistent with the sedimentation-velocity AUC results. We conclude that the species corresponding to sedimentation coefficients of 1.6 and 2.4 S are the H-NS<sub>1-83</sub> C21S dimer and tetramer, respectively. However, our analysis does not exclude the presence of minor populations of higher order oligomers (such as hexamers). The AUC analysis provides the first evidence using a shape-independent technique that the H-NS oligomerization domain forms a homotetramer under solution conditions.

Why does self-association of the oligomerization domain appear to halt at the formation of the tetrameric species? Assuming the model of the parallel coiled coil in which the oligomerization process occurs using an interface whereby one dimer abuts another (as proposed by Esposito *et al.*, 2002), the formation of higher order complexes has to be an anticooperative process under these low ionic strength condi-

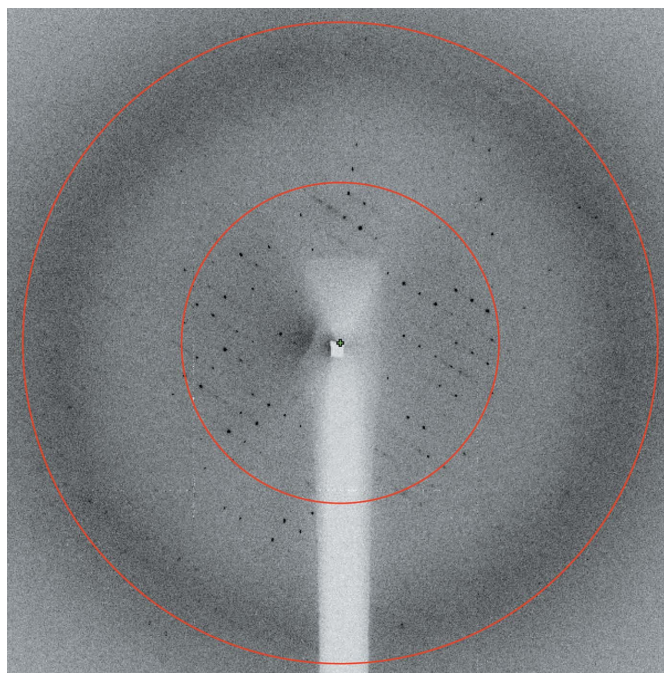


**Figure 2**

A X-ray diffraction-pattern image collected on European Synchrotron Radiation Facility beamline ID23-2 from a native H-NS<sub>1-83</sub> C21S crystal; the X-ray wavelength used was 0.873 Å, the crystal-to-detector distance was set to 371.05 mm and the image was collected over  $1^\circ$  oscillations with an exposure time of 2 s. Resolution rings at 8 and 4 Å are indicated by red circles.

tions. Since this is not observed in the presence of inorganic salt concentrations, where concentration-dependent large oligomers can prevail, this is likely to result from the net charge on the interacting species. The calculated charge of the H-NS<sub>1-83</sub> C21S protein (including the GSH residues left over from the His tag) at pH 7.0 is -6.105 (calculated from the amino-acid sequence using *SEDNTERP*). Thus, self-association would increase the net charge on the interacting species (dimers and tetramers), making molecular repulsion a significant driving force precluding oligomer formation. This charge effect is shielded in buffers with higher salt concentrations.

### 3.2. Crystallization of H-NS<sub>1-83</sub> C21S

Hampton Research and Emerald BioStructures sparse-matrix crystallization screens failed to identify any suitable crystallization conditions for H-NS<sub>1-83</sub> C21S. The absence of protein crystals is likely to be the result of the salt present in many of the crystallization buffers, as an increase in the salt concentration increases the heterogeneity of the H-NS<sub>1-83</sub> C21S protein solution (Leonard *et al.*, 2009). Therefore, a crystallization screen in which the pH and precipitant were varied without any additional inorganic salt was prepared to keep the ionic strength to a minimum. Using this crystallization screen, two different crystal forms were identified for H-NS<sub>1-83</sub> C21S after two weeks of incubation at 289 K. Hexagonal-based pyramid-shaped crystals were identified from hanging-drop or microbatch setups in drops containing a 1:1 mixture of the H-NS<sub>1-83</sub> C21S solution with a solution containing 100 mM MES pH 6.0 with 10–30% (v/v) 2-methyl-2,4-pentanediol or 10–20% (v/v) PEG 400. Whiskers of H-NS<sub>1-83</sub> C21S crystals were also identified in conditions at pH 8.0–9.0 containing 10–20% (w/v) PEG 2000, PEG 4000 or PEG 6000. Additive screening (Molecular Dimensions Additive Screen I) identified phenol as a useful additional component of the crystallization conditions. The best crystals identified were grown from a mixture of 1 µl 2 mM H-NS<sub>1-83</sub> C21S in 10 mM MOPS pH 7.0 with 1 µl 100 mM MES, 20% (v/v) MPD and 20 mM phenol pH 6.2 using the microbatch setup. A complete 4 Å resolution data set consisting of 75 images was collected from a native H-NS<sub>1-83</sub> C21S crystal on ESRF beamline ID23\_2 (Fig. 2). Data-collection statistics are given in Table 1. Data analysis using *POINTLESS* (Evans, 2006) established the Laue group as *P6/m* (probability score of 0.993), with the equivalent space groups *P6<sub>1</sub>* and *P6<sub>5</sub>* being the most likely space groups (confidence score of 0.837). Based on space group *P6<sub>1</sub>* or *P6<sub>5</sub>*, the algorithm used by the *Matthews Probability Calculator* (Kantardjiev & Rupp, 2003) calculated a most likely Matthews coefficient  $V_M$  (Matthews, 1968) of 2.3 Å<sup>3</sup> Da<sup>-1</sup> (81% probability), which is consistent with the presence of six H-NS<sub>1-83</sub> C21S monomers in the asymmetric unit with 47% solvent content. These molecules are likely to be in the form of three H-NS<sub>1-83</sub> C21S homodimers, although the presence of a single homotetramer in the asymmetric unit ( $V_M$  of 3.8 Å<sup>3</sup> Da<sup>-1</sup> and 64% solvent content) cannot be ruled out. This scenario was the second most likely (9.8%) according to the *Matthews Probability Calculator*.

While the structural basis for auto-assembly might already be apparent from 4 Å data, such an analysis would certainly profit from improved resolution. In view of this, we are currently testing different cryocooling conditions. We are also pursuing crystal-dehydration methods (Heras & Martin, 2005; Petock *et al.*, 2001) in order to improve the diffraction resolution of the crystals. Additionally, constructs have also been prepared that trim two or three amino acids from the N-terminus or C-terminus of the protein to remove potential flexible chains that might be preventing closer crystal packing from taking place. A refined three-dimensional structure of the complete

**Table 1**

Data-collection and refinement statistics.

Values in parentheses are for the highest resolution shell.

Crystal system, space group	Hexagonal, <i>P6<sub>1</sub></i> or <i>P6<sub>5</sub></i>
Unit-cell parameters (Å)	$a = b = 130.53$ , $c = 55.11$
Diffraction source	ESRF ID23-2
Temperature (K)	105
Wavelength (Å)	0.873
Resolution range (Å)	32.63–4.00 (4.14–4.00)
Completeness (%)	97.4 (97.6)
Multiplicity	2.77 (2.53)
$\langle I/\sigma(I) \rangle$	8.3 (2.7)
$R_{\text{merge}}^{\dagger}$	0.066 (0.336)
Matthews coefficient $V_M^{\ddagger}$ (Å <sup>3</sup> Da <sup>-1</sup> )	2.5 [3.75]

<sup>†</sup>  $R_{\text{merge}} = \frac{\sum_{hkl} \sum_i |I_i(hkl) - \langle I(hkl) \rangle|}{\sum_{hkl} \sum_i I_i(hkl)}$ , where  $I_i(hkl)$  and  $\langle I(hkl) \rangle$  are the observed individual and mean intensities of a reflection with indices  $hkl$ , respectively,  $\sum_i$  is the sum over the individual measurements of a reflection with indices  $hkl$  and  $\sum_{hkl}$  is the sum over all reflections. <sup>‡</sup> Estimated assuming the presence of six molecules in the asymmetric unit; the value in square brackets is for four molecules in the asymmetric unit.

H-NS oligomerization domain would provide an important insight into how this protein is able to associate to form higher order oligomeric complexes both with itself and with homologous proteins such as StpA (Johansson *et al.*, 2001) and Hha (Nieto *et al.*, 2002).

This work was funded by a BBSRC fully funded studentship to PGL. We would like to thank Dr Ajit Basak for kindly collecting the X-ray diffraction data at the European Synchrotron Radiation Facility and Dr Snezana Djordjevic for access to crystallization equipment.

### References

- Bloch, V., Yang, Y., Margeat, E., Chavanieu, A., Auge, M. T., Robert, B., Arold, S., Rimsky, S. & Kochoyan, M. (2003). *Nature Struct. Biol.* **10**, 212–218.
- Browning, D. F., Cole, J. A. & Busby, S. J. (2000). *Mol. Microbiol.* **37**, 1258–1269.
- Dame, R. T. & Goosen, N. (2002). *FEBS Lett.* **529**, 151–156.
- De la Cruz, M. A., Fernandez-Mora, M., Guadarrama, C., Flores-Valdez, M. A., Bustamante, V. H., Vazquez, A. & Calva, E. (2007). *Mol. Microbiol.* **66**, 727–743.
- Dorman, C. J. (2004). *Nature Rev. Microbiol.* **2**, 391–400.
- Dorman, C. J., Hinton, J. C. & Free, A. (1999). *Trends Microbiol.* **7**, 124–128.
- Esposito, D., Petrovic, A., Harris, R., Ono, S., Eccleston, J. F., Mbabaali, A., Haq, I., Higgins, C. F., Hinton, J. C., Driscoll, P. C. & Ladbury, J. E. (2002). *J. Mol. Biol.* **324**, 841–850.
- Evans, P. (2006). *Acta Cryst.* **D62**, 72–82.
- Falconi, M., Prosseda, G., Giangrossi, M., Beghetto, E. & Colonna, B. (2001). *Mol. Microbiol.* **42**, 439–452.
- Heras, B. & Martin, J. L. (2005). *Acta Cryst.* **D61**, 1173–1180.
- Hommais, F., Krin, E., Laurent-Winter, C., Soutourina, O., Malpertuy, A., Le Caer, J.-P., Danchin, A. & Bertin, P. (2001). *Mol. Microbiol.* **40**, 20–36.
- Johansson, J., Eriksson, S., Sonden, B., Wai, S. N. & Uhlin, B. E. (2001). *J. Bacteriol.* **183**, 2343–2347.
- Kantardjiev, K. A. & Rupp, B. (2003). *Protein Sci.* **12**, 1865–1871.
- Laue, T. M., Shah, B. D., Ridgeway, T. M. & Pelletier, S. L. (1992). *Analytical Ultracentrifugation in Biochemistry and Polymer Science*, edited by S. E. Harding, A. J. Rowe & J. Horton, pp. 90–125. Cambridge: Royal Society of Chemistry.
- Leonard, P. G., Ono, S., Gor, J., Perkins, S. J. & Ladbury, J. E. (2009). *Mol. Microbiol.* **73**, 165–179.
- Matthews, B. W. (1968). *J. Mol. Biol.* **33**, 491–497.
- Nieto, J. M., Madrid, C., Miquelay, E., Parra, J.-L., Rodriguez, S. & Juarez, A. (2002). *J. Bacteriol.* **184**, 629–635.
- Ono, S., Goldberg, M. D., Olsson, T., Esposito, D., Hinton, J. C. & Ladbury, J. E. (2005). *Biochem. J.* **391**, 203–213.
- Petock, J. M., Wang, Y.-F., DuBois, G. C., Harrison, R. W. & Weber, I. T. (2001). *Acta Cryst.* **D57**, 763–765.
- Pflugrath, J. W. (1999). *Acta Cryst.* **D55**, 1718–1725.

- Rimsky, S. (2004). *Curr. Opin. Microbiol.* **7**, 109–114.
- Schuck, P. (2000). *Biophys. J.* **78**, 1606–1619.
- Smyth, C. P., Lundback, T., Renzoni, D., Siligardi, G., Beavil, R., Layton, M., Sidebotham, J. M., Hinton, J. C., Driscoll, P. C., Higgins, C. F. & Ladbury, J. E. (2000). *Mol. Microbiol.* **36**, 962–972.
- White-Ziegler, C. A. & Davis, T. R. (2009). *J. Bacteriol.* **191**, 1106–1110.
- Williamson, H. S. & Free, A. (2005). *Mol. Microbiol.* **55**, 808–827.